



Synthesis and Performance Evaluation of $Ba_xSr_{1-x}TiO_3$ Ceramic-Based MIM Capacitor for Energy Storage Application

Smitha P. S., Jitha S. Jayan, Appukuttan Saritha, V. Suresh Babu & Shiny G.

To cite this article: Smitha P. S., Jitha S. Jayan, Appukuttan Saritha, V. Suresh Babu & Shiny G. (2020) Synthesis and Performance Evaluation of $Ba_xSr_{1-x}TiO_3$ Ceramic-Based MIM Capacitor for Energy Storage Application, Integrated Ferroelectrics, 212:1, 177-189, DOI: [10.1080/10584587.2020.1819032](https://doi.org/10.1080/10584587.2020.1819032)

To link to this article: <https://doi.org/10.1080/10584587.2020.1819032>



Published online: 11 Nov 2020.



Submit your article to this journal [↗](#)



Article views: 25








View related articles [↗](#)



View Crossmark data [↗](#)



Synthesis and Performance Evaluation of $Ba_xSr_{1-x}TiO_3$ Ceramic-Based MIM Capacitor for Energy Storage Application

Smitha P. S.^a , Jitha S. Jayan^b , Appukuttan Saritha^b , V. Suresh Babu^c , and Shiny G.^d 

^aDepartment of Electronics and Communication Engineering, College of Engineering Trivandrum, APJ Abdul Kalam Technological University, Kerala, India; ^bDepartment of Chemistry, Amrita School of Arts & Sciences, Amrita Vishwa Vidyapeetham, Amritapuri Campus, Kollam, Kerala, India; ^cDepartment of Electronics and Communication Engineering, Government Engineering College Wayanad, APJ Abdul Kalam Technological University, Kerala, India; ^dDepartment of Electronics and Communication Engineering, Government Engineering College Kannur, APJ Abdul Kalam Technological University, Kerala, India

ABSTRACT

Metal-insulator-metal (MIM) capacitor with high- k insulator such as BST enhances specific capacitance. The effects of barium mole fraction (x) of $Ba_xSr_{1-x}TiO_3$ ceramic-based MIM capacitor on specific capacitance and leakage current density are reported in this article. $Ba_xSr_{1-x}TiO_3$ nanopowder for various x are synthesized using solid-state reaction method and the performance parameters of Ag/ $Ba_xSr_{1-x}TiO_3$ /Ag MIM capacitors are evaluated. The mean crystallite sizes are in 20 to 60 nm range. $Ba_{0.7}Sr_{0.3}TiO_3$ ceramics show higher relative permittivity owing to its higher mean crystallite size. The insulator with higher crystallite size at dominant orientation shows enhanced leakage performance. $Ba_{0.1}Sr_{0.9}TiO_3$ ceramic capacitor shows optimum performance altogether.

ARTICLE HISTORY

Received 8 April 2020
Accepted 12 July 2020

KEYWORDS

Energy storage; ceramic capacitor; crystallite size; specific capacitance; leakage current

1. Introduction

Barium strontium titanate is a continuous solid solution of barium titanate and strontium titanate and is the best ferroelectric material for applications in multilayer ceramic capacitors, ferroelectric random access memories (FRAM), microwave phase shifters, tunable filters, opto-electronic devices and sensors owing to its high dielectric constant, small dielectric loss, high breakdown field strength, pyroelectric properties, ferroelectricity and good thermal stability [1–6]. These peculiar properties of $Ba_xSr_{1-x}TiO_3$ make it suitable for considering in energy storage devices. Metal-insulator-metal (MIM) capacitors (electrostatic capacitors) are best choice for energy storage devices owing to fast charging–discharging characteristics and very high life-span [7]. Being a very good dielectric material, $Ba_xSr_{1-x}TiO_3$ is one of the best candidates for insulator in metal-insulator-metal capacitors.

The critical performance parameters of MIM capacitors in energy storage application are specific capacitance and leakage current. Specific capacitance enhancement of MIM capacitor can be achieved by using $\text{Ba}_x\text{Sr}_{1-x}\text{TiO}_3$ as insulator material on account of its high relative permittivity [8]. The leakage current performance can also be improved by synthesizing $\text{Ba}_x\text{Sr}_{1-x}\text{TiO}_3$ sample with suitable barium mole fraction. Barium strontium titanate have been synthesized by numerous techniques namely solid-state reaction [9,10], hydrothermal [11,12], sol-gel [13–15], spray pyrolysis [16] and RF magnetron sputtering [17,18].

In this work, the $\text{Ba}_x\text{Sr}_{1-x}\text{TiO}_3$ samples were prepared from barium carbonate, strontium carbonate and titanium dioxide using conventional solid-state reaction technique only, but at lower thermal budget and synthesis process duration. $\text{Ba}_x\text{Sr}_{1-x}\text{TiO}_3$ nanopowder samples for different barium mole fractions $x=0.1, 0.3, 0.5, 0.7$ and 0.9 were synthesized. Further green pellets of each sample were made using Carver auto series automatic hydraulic laboratory press with enhanced “NE” digital control system. Furthermore silver is painted on both sides of sintered pellets after polishing to form $\text{Ag}/\text{Ba}_x\text{Sr}_{1-x}\text{TiO}_3/\text{Ag}$ MIM capacitors and then evaluated specific capacitance and leakage current density.

2. Experimental Procedure

The $\text{Ba}_x\text{Sr}_{1-x}\text{TiO}_3$ nanopowder was synthesized using barium carbonate (ACS reagent grade, 99%, Spectrum), strontium carbonate (ACS reagent grade, 99%, Spectrum) and titanium dioxide (ACS reagent grade, 98%, Spectrum) as precursors for barium, strontium and titanium, respectively. Stoichiometric proportions of barium carbonate and titanium oxide nanopowders were blended in agate mortar for 1 h. Similarly Stoichiometric proportions of strontium carbonate and titanium oxide nanopowders were blended in agate mortar for 1 h. Further calcining both mixtures at 1100°C for 4 h was carried out. The melts were taken out and blended in agate mortar for 1 h which result in barium titanate and strontium titanate powders. Stoichiometric proportions of barium titanate and strontium titanate powders were mixed well in agate mortar for 1 h, and then, calcining the blend at 1100°C for 4 h resulted in $\text{Ba}_x\text{Sr}_{1-x}\text{TiO}_3$ nanopowder.

$\text{Ba}_x\text{Sr}_{1-x}\text{TiO}_3$ nanopowder was mixed with 4 wt% aqueous poly vinyl alcohol, the binder in agate mortar for 15 min and then dried up in hot air oven at 60°C for 20 min. The mixture was taken out and blended again in agate mortar for 15 min. Further the powder was die-pressed into pellets using Carver auto series automatic hydraulic laboratory press with enhanced “NE” digital control system having 11 mm diameter die at 1 ton pressure. The green pellets were then sintered at 1275°C for 2 h in Nabertherm sintering furnace. The $\text{Ba}_x\text{Sr}_{1-x}\text{TiO}_3$ nanopowder with $x=0.1, 0.3, 0.5, 0.7$ and 0.9 were prepared and made into pellets using the above said procedure. The mass, diameter and thickness of each pellet were measured and noted after polishing.

Furthermore silver metal paste was spread over top and bottom surfaces of pellets to act as top and bottom electrodes of MIM capacitor device and kept at 130°C for 15 min in hot air oven. The electrical continuity of the electrode surfaces were verified using a multimeter. For capacitor leads, copper wires were fixed at top and bottom electrodes with silver paste and dried at 130°C for 15 min in hot air oven.

The capacitance and dielectric constant were measured using Hioki 3532-50 LCR Hi-Tester. The leakage current was measured using IV meter. X-ray powder diffraction patterns were observed using Bruker D8 Advance equipment.

3. Results and Discussion

The performance evaluation of $\text{Ba}_x\text{Sr}_{1-x}\text{TiO}_3$ ceramic-based Metal-Insulator-Metal capacitor for different barium mole fractions (x) is discussed in this section.

3.1. Specific Capacitance

During sintering each green pellet undergoes different area shrinkage according to material contents. Hence, it is better to evaluate specific capacitance rather than capacitance density. Specific capacitance is simply capacitance per unit mass. Figure 1 shows the specific capacitance of $\text{Ba}_x\text{Sr}_{1-x}\text{TiO}_3$ ceramic-based MIM capacitor for $x = 0.1, 0.3, 0.5, 0.7, 0.9$ and 1.0 . From Figure 1, it is evident that $\text{Ba}_{0.7}\text{Sr}_{0.3}\text{TiO}_3$ ceramic-based MIM capacitor possesses high specific capacitance and can be used to store more electrical energy.

Relative permittivity can also be measured using LCR meter. Since the specific capacitance is stabilized at a frequency of about 1 MHz, the relative permittivity of $\text{Ba}_x\text{Sr}_{1-x}\text{TiO}_3$ ceramic-based MIM capacitor for $x = 0.1, 0.3, 0.5, 0.7, 0.9$ and 1.0 at 1 MHz are measured and is shown in Figure 2. It is obvious from Figure 1 that $\text{Ba}_{0.7}\text{Sr}_{0.3}\text{TiO}_3$ ceramic-based MIM capacitor possesses high relative permittivity.

The enhanced specific capacitance, and hence, energy storage capacity of $\text{Ba}_{0.7}\text{Sr}_{0.3}\text{TiO}_3$ ceramic-based MIM capacitor is having direct dependence on mean crystallite size of $\text{Ba}_{0.7}\text{Sr}_{0.3}\text{TiO}_3$ sample and is explained in subsection 3.3.

3.2. Leakage Current Density

Leakage current density versus bias voltage is shown in Figure 3. The leakage current performance enhances as barium mole fraction decreases except for $x = 0.5$. It is observed that $\text{Ba}_{0.5}\text{Sr}_{0.5}\text{TiO}_3$ ceramic-based MIM capacitor shows slight improvement in leakage current performance contrary to expected result. The measured leakage current density of $\text{Ba}_x\text{Sr}_{1-x}\text{TiO}_3$ ceramic-based MIM capacitor for $x = 0.1, 0.3, 0.5, 0.7, 0.9$ and 1.0 at 1 V are 7.24×10^{-10} A/cm², 5.44×10^{-9} A/cm², 2.91×10^{-9} A/cm², 1.46×10^{-8} A/cm², 3.24×10^{-8} A/cm² and 9.87×10^{-8} A/cm², respectively.

The pellets are of different thickness, and hence, it is better to analyze leakage current density variation with electric field rather than bias voltage. Figure 4 shows leakage current density against electric field of $\text{Ba}_x\text{Sr}_{1-x}\text{TiO}_3$ ceramic-based MIM capacitor for different barium mole fraction. The average thickness of pellets is about 2 mm, and hence, bias voltage of 1 V corresponds to electric field of 5 V/cm. The measured leakage current density of $\text{Ba}_x\text{Sr}_{1-x}\text{TiO}_3$ ceramic-based MIM capacitor for $x = 0.1, 0.3, 0.5, 0.7, 0.9$ and 1.0 at 5 V/cm are 6.64×10^{-10} A/cm², 4.32×10^{-9} A/cm², 3.48×10^{-9} A/cm², 1.41×10^{-8} A/cm², 3.61×10^{-8} A/cm² and 7.47×10^{-8} A/cm², respectively. It is observed

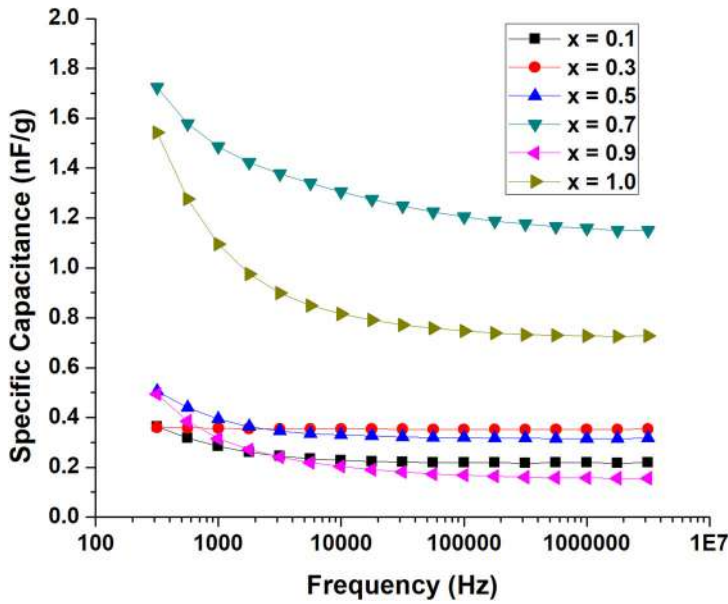


Figure 1. Specific capacitance of $\text{Ba}_x\text{Sr}_{1-x}\text{TiO}_3$ ceramic-based MIM capacitor for $x=0.1, 0.3, 0.5, 0.7, 0.9$ and 1.0 .

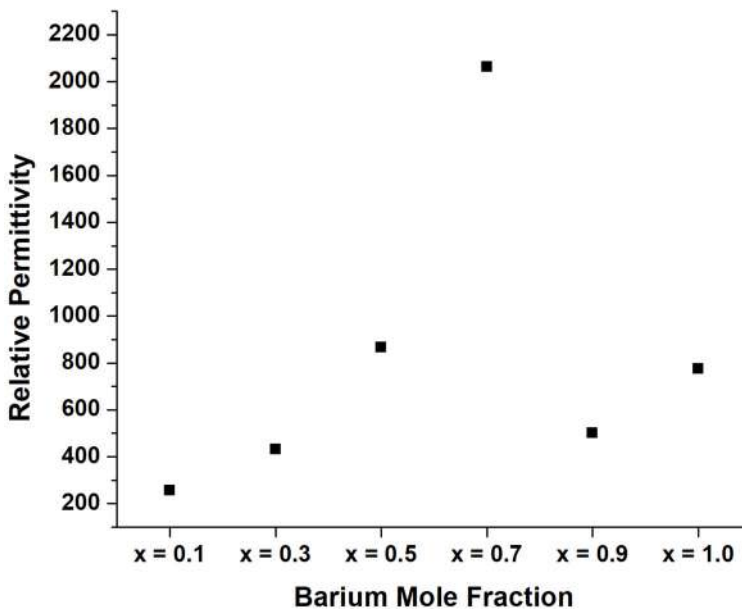


Figure 2. Relative permittivity of $\text{Ba}_x\text{Sr}_{1-x}\text{TiO}_3$ ceramic-based MIM capacitor for $x=0.1, 0.3, 0.5, 0.7, 0.9$ and 1.0 at 1 MHz .

that the change in measured leakage current densities with respect to bias voltage and corresponding electric field is marginal.

It is evident from [Figure 4](#) that leakage current performance is achieved in $\text{Ba}_{0.1}\text{Sr}_{0.9}\text{TiO}_3$ ceramic-based MIM capacitor is better compared to that with other barium mole fractions. The enhanced leakage current performance of $\text{Ba}_{0.1}\text{Sr}_{0.9}\text{TiO}_3$ ceramic-based

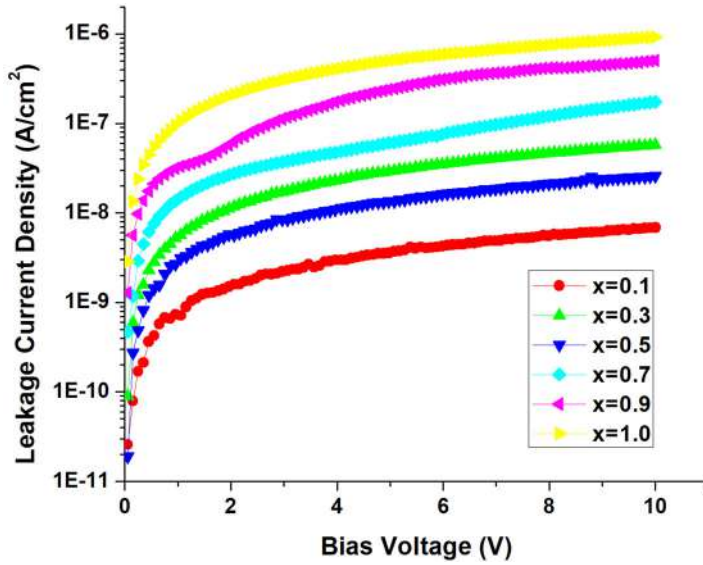


Figure 3. Leakage current density versus bias voltage of $\text{Ba}_x\text{Sr}_{1-x}\text{TiO}_3$ ceramic-based MIM capacitor for $x = 0.1, 0.3, 0.5, 0.7, 0.9$ and 1.0 .

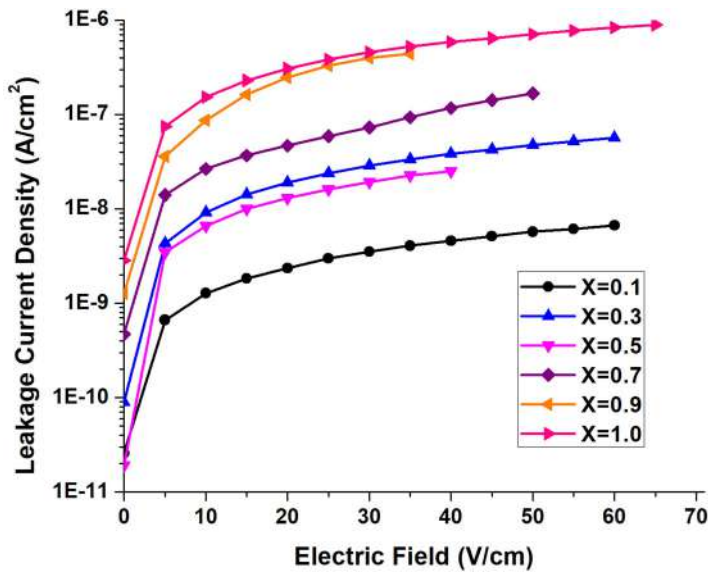


Figure 4. Leakage current density versus electric field of $\text{Ba}_x\text{Sr}_{1-x}\text{TiO}_3$ ceramic-based MIM capacitor for $x = 0.1, 0.3, 0.5, 0.7, 0.9$ and 1.0 .

MIM capacitor has direct dependence on crystallite size of $\text{Ba}_{0.1}\text{Sr}_{0.9}\text{TiO}_3$ sample and is discussed in subsection 3.3.

3.3. X-Ray Powder Diffraction

The specific capacitance and leakage current performance variation with barium mole fraction can be studied using X-ray powder diffraction pattern. XRD patterns of $\text{Ba}_x\text{Sr}_{1-x}$

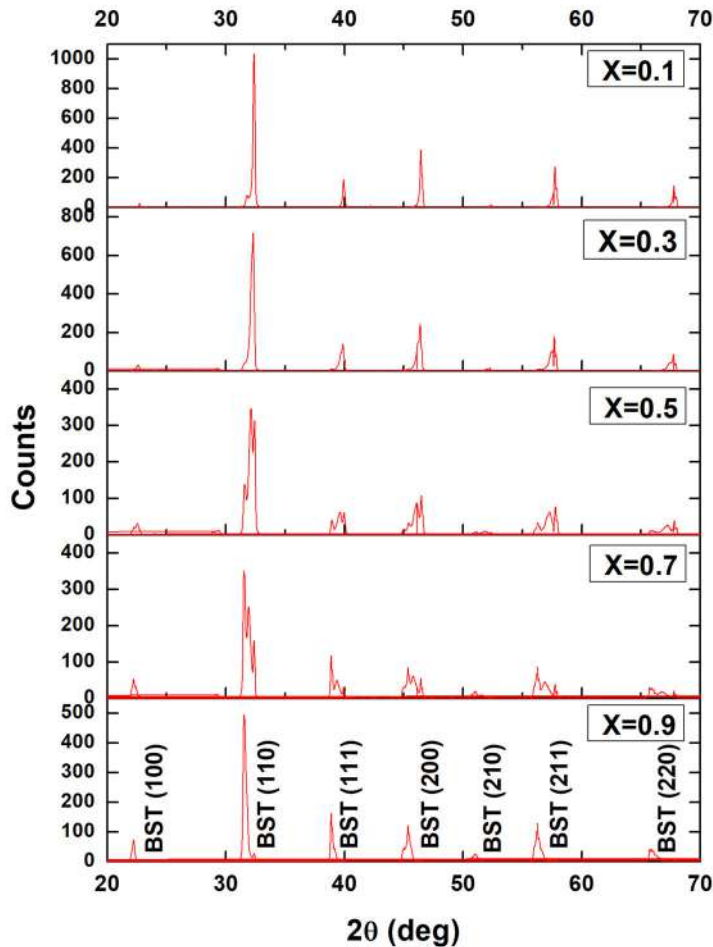


Figure 5. X-ray powder diffraction pattern of $\text{Ba}_x\text{Sr}_{1-x}\text{TiO}_3$ ceramic-based MIM capacitor for $x = 0.1, 0.3, 0.5, 0.7$ and 0.9 .

$_{-x}\text{TiO}_3$ nanopowder for barium mole fraction, $x = 0.1, 0.3, 0.5, 0.7$ and 0.9 are shown in [Figure 5](#). The diffraction peaks are observed at angles $2\theta = 22^\circ, 32^\circ, 40^\circ, 46.5^\circ, 52^\circ, 58^\circ$ and 68° correspond to BST(100), BST(110), BST(111), BST(200), BST(210), BST(211) and BST(220), respectively [19–21]. It is also evident from [Figure 5](#) that the prepared samples do not possess any diffraction peaks from impurity phases.

The diffraction peaks corresponding to BST(110) of $\text{Ba}_x\text{Sr}_{1-x}\text{TiO}_3$ nanopowder are higher in all barium mole fractions compared to other orientations of BST such as 100, 111, 200, 210, 211 and 220 [22–24]. It can be observed from [Figure 5](#) that the intensity of diffraction peak of $\text{Ba}_{0.1}\text{Sr}_{0.9}\text{TiO}_3$ nanopowder at 110 plane is higher compared to that of $\text{Ba}_x\text{Sr}_{1-x}\text{TiO}_3$ nanopowder with remaining mole fractions. This indicates that the $\text{Ba}_{0.1}\text{Sr}_{0.9}\text{TiO}_3$ nanopowder sample attained better crystallinity which justifies lower leakage current [21] in $\text{Ba}_{0.1}\text{Sr}_{0.9}\text{TiO}_3$ -based MIM capacitor ([Figure 4](#)).

The crystallite size can be estimated from X-ray powder diffraction pattern using Debye–Scherrer equation [25].

Table 1. Crystallite size and lattice parameter of $\text{Ba}_x\text{Sr}_{1-x}\text{TiO}_3$ nanopowder for $x = 0.1, 0.3, 0.5, 0.7$ and 0.9 at dominant planes of reflection using X-ray spectrum analysis.

x	2θ (deg)	FWHM (deg)	Crystallite size (nm)	hkl	d_{hkl} (Å)	Lattice parameter (Å)
0.1	22.7346	0.1986	40.3648	100	3.9082	3.9082
	32.3806	0.1977	41.4057	110	2.7626	3.9069
	39.9440	0.2160	38.7090	111	2.2552	3.9062
	46.4670	0.2340	36.5522	200	1.9527	3.9054
	57.7627	0.2520	35.6120	211	1.5948	3.9065
	67.8212	0.2856	33.1521	220	1.3807	3.9053
0.3	22.5935	0.2968	27.0008	100	3.9323	3.9323
	32.2470	0.3315	24.6773	110	2.7738	3.9227
	39.7987	0.3833	21.8090	111	2.2631	3.9199
	46.3085	0.4094	20.8810	200	1.9590	3.9180
	57.5834	0.4995	17.9513	211	1.5994	3.9176
	67.5967	0.5106	18.5189	220	1.3848	3.9167
0.5	22.4580	0.5419	14.7878	100	3.9557	3.9557
	32.2154	0.5883	13.9059	110	2.7764	3.9264
	39.5771	0.3151	26.5105	111	2.2753	3.9409
	46.0439	0.3524	24.2347	200	1.9697	3.9393
	57.8265	0.2004	44.8006	211	1.5932	3.9026
	67.8447	0.1259	75.2426	220	1.3803	3.9041
0.7	22.2744	0.4096	19.5577	100	3.9879	3.9879
	31.6499	0.4002	20.4113	110	2.8247	3.9948
	38.9186	0.1641	50.8022	111	2.3123	4.0050
	46.4542	0.1002	85.3672	200	1.9532	3.9064
	57.7585	0.0968	92.6762	211	1.5949	3.9068
	67.7867	0.0924	102.5016	220	1.3813	3.9070
0.9	22.2132	0.2788	28.7281	100	3.9987	3.9987
	31.6011	0.3181	25.6769	110	2.8290	4.0008
	38.9266	0.2206	37.7790	111	2.3118	4.0042
	45.3782	0.1965	43.3488	200	1.9970	3.9940
	56.2870	0.3905	22.8231	211	1.6331	4.0002
	65.9977	0.6733	13.9174	220	1.4144	4.0005

$$\text{Crystallite size} = \frac{k \times \lambda}{\text{FWHM} \times \cos \theta} \quad (1)$$

where $k = 0.89$ (shape factor), $\lambda = 0.15406$ nm (wavelength of X-ray), FWHM is width of diffraction peak at half of maximum intensity of that peak measured in radians and θ is half of diffraction angle.

The interplane spacing (d_{hkl}) can be computed using Bragg's law [26] which is given as

$$d_{hkl} = \frac{\lambda}{2 \times \sin \theta} \quad (2)$$

where $h k l$ is miller indices of Bragg plane which indicates internal plane of a crystal.

The equation for a cubic crystal [27] is

$$\sin^2 \theta = \frac{\lambda^2 \times (h^2 + k^2 + l^2)}{4 \times a^2} \quad (3)$$

The equation for lattice parameter as a function of interplane spacing and miller indices can be derived using Eqs. (2) and (3) which is given as

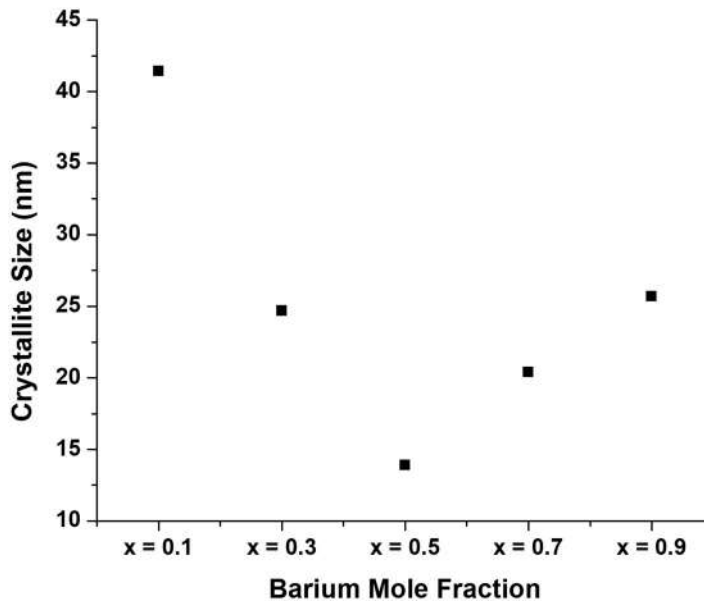


Figure 6. Crystallite sizes of $\text{Ba}_x\text{Sr}_{1-x}\text{TiO}_3$ ceramic-based MIM capacitor for $x = 0.1, 0.3, 0.5, 0.7$ and 0.9 at dominant orientation.

$$\text{LatticeParameter} = d_{hkl} \times \sqrt{(h^2 + k^2 + l^2)} \quad (4)$$

The crystallite sizes and lattice parameters of $\text{Ba}_x\text{Sr}_{1-x}\text{TiO}_3$ nanopowder for $x = 0.1, 0.3, 0.5, 0.7$ and 0.9 at dominant planes of reflection computed using Eqs. (1) and (4) and is given in Table 1.

The crystallite sizes at dominant orientation of $\text{Ba}_x\text{Sr}_{1-x}\text{TiO}_3$ nanopowder for $x = 0.1, 0.3, 0.5, 0.7$ and 0.9 are shown in Figure 6. The highest grain size is achieved in $\text{Ba}_{0.1}\text{Sr}_{0.9}\text{TiO}_3$ nanopowder sample and is due to lower XRD pattern broadening at 110 plane. This again indicates sharper XRD pattern and better crystallinity achieved in the $\text{Ba}_{0.1}\text{Sr}_{0.9}\text{TiO}_3$ nanopowder sample which leads to enhanced leakage current performance.

The average crystallite sizes of samples prepared are in the range of 20 to 60 nm and is comparable with that obtained in the previously reported research works using complex synthesis methods [1,2,4,6,28]. Insulator materials with higher mean crystallite size shows increased relative permittivity [29]. Figure 7 shows that $\text{Ba}_{0.7}\text{Sr}_{0.3}\text{TiO}_3$ sample possesses higher average crystallite size and this substantiate the enhanced specific capacitance of $\text{Ba}_{0.7}\text{Sr}_{0.3}\text{TiO}_3$ ceramic-based MIM capacitor discussed in subsection 3.1.

It is evident from Table 1 that the lattice parameter of $\text{Ba}_x\text{Sr}_{1-x}\text{TiO}_3$ sample increases as barium mole fraction (x) increases. This increase in lattice parameter is due to the larger ionic radius of Ba^{2+} than that of Sr^{2+} [30].

3.4. Performance Evaluation

Specific capacitance and leakage current are equally important as far as an energy storage device concerned. For the best energy storage device, specific capacitance should be

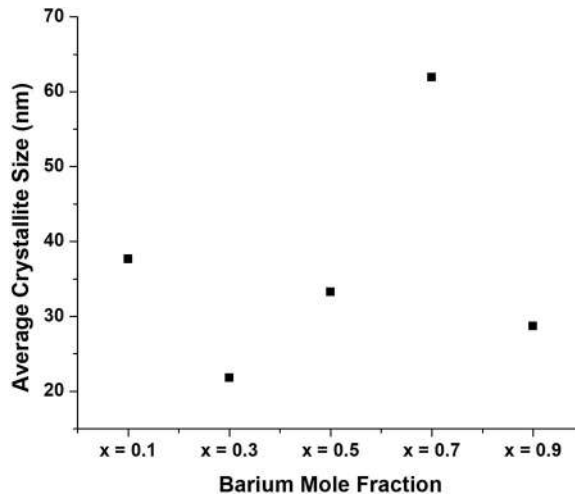


Figure 7. Average Crystallite sizes of $\text{Ba}_x\text{Sr}_{1-x}\text{TiO}_3$ ceramic-based MIM capacitor for $x = 0.1, 0.3, 0.5, 0.7$ and 0.9 .

maximum and leakage current should be minimum. Hence, the performance of proposed $\text{Ba}_x\text{Sr}_{1-x}\text{TiO}_3$ ceramic-based MIM capacitor for $x = 0.1, 0.3, 0.5, 0.7, 0.9$ and 1.0 can be evaluated with specific capacitance – leakage current ratio. It is defined as the ratio of specific capacitance at a frequency of 1 MHz and leakage current density at an electric field of 5 V/cm . The MIM capacitor with highest value of specific capacitance – leakage current ratio is the one shows optimum performance.

It is evident from [Figure 8](#) that $\text{Ba}_{0.1}\text{Sr}_{0.9}\text{TiO}_3$ ceramic-based MIM capacitor shows optimum performance.

3.5. Synthesis and Performance Comparison with Related Research Works

[Table 2](#) gives the comparison of synthesis parameters namely insulator material, synthesis technique, calcining and sintering temperatures as well as performance parameters in particular relative permittivity and leakage current density of $\text{Ag}/\text{Ba}_x\text{Sr}_{1-x}\text{TiO}_3/\text{Ag}$ ceramic-based MIM capacitor proposed in this article with previous research works. The sample synthesis method followed in this work is very simple compared to other related works. The calcination and sintering of prepared samples are done with efficient temperature budget.

Specific capacitances are not mentioned in any of the related works given in [Table 2](#), and hence, the comparison is limited to relative permittivity which is directly proportional to specific capacitance. The relative permittivity of $\text{Ba}_{0.7}\text{Sr}_{0.3}\text{TiO}_3$ sample prepared in this work is better compared to other related works. Choi *et al.* [28] achieved much better relative permittivity with $\text{Ba}_{0.7}\text{Sr}_{0.3}\text{TiO}_3$ sample compared to our work at the expense of complex synthesis method. The leakage current study has not been done in many related research works. It is evident from [Table 2](#) that the leakage current density of proposed $\text{Ag}/\text{Ba}_x\text{Sr}_{1-x}\text{TiO}_3/\text{Ag}$ ceramic-based MIM capacitor is very low compared to other related works [6,14].

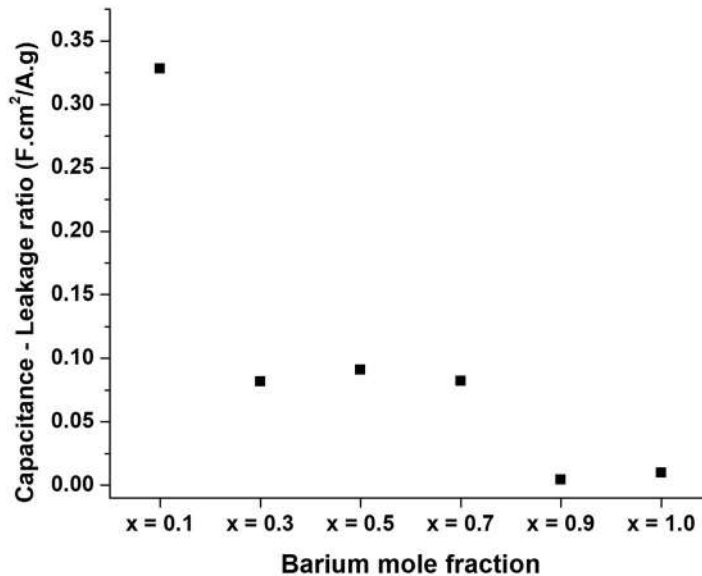


Figure 8. Specific capacitance - leakage current ratio $Ba_xSr_{1-x}TiO_3$ ceramic-based MIM capacitor for $x = 0.1, 0.3, 0.5, 0.7, 0.9$ and 1.0 .

4. Conclusion

The effects of varying barium mole fraction (x) of $Ba_xSr_{1-x}TiO_3$ ceramic-based MIM capacitor on specific capacitance and leakage current density are reported in this article. It is observed that $Ba_{0.7}Sr_{0.3}TiO_3$ ceramic-based MIM capacitor shows higher relative permittivity, and hence, higher specific capacitance compared to $Ba_xSr_{1-x}TiO_3$ ceramic-based MIM capacitors with other barium mole fractions. It is also observed that the leakage current decreases as barium mole fraction decreases except for $x = 0.5$ which shows slight improvement in leakage current performance in contrast to the expected result. The leakage current density of $Ba_{0.1}Sr_{0.9}TiO_3$ ceramic-based MIM capacitor is lower compared to $Ba_xSr_{1-x}TiO_3$ ceramic-based MIM capacitor with other barium mole fractions.

The increased specific capacitance of $Ba_{0.7}Sr_{0.3}TiO_3$ ceramic-based MIM capacitor and enhanced leakage current performance of $Ba_{0.1}Sr_{0.9}TiO_3$ ceramic-based MIM capacitor are explained with X-ray powder diffraction pattern analysis. It is observed that higher mean crystallite size results in increased relative permittivity and sharper diffraction peak at dominant orientation, which leads to enhanced leakage current. Hence, higher relative permittivity of $Ba_{0.7}Sr_{0.3}TiO_3$ ceramic-based MIM capacitor possesses higher energy storage capacity due to its higher mean crystallite size and $Ba_{0.1}Sr_{0.9}TiO_3$ ceramic-based MIM capacitor can hold stored electrical energy for a long duration due to its higher crystallite size at dominant orientation. Further $Ba_{0.1}Sr_{0.9}TiO_3$ ceramic-based MIM capacitor is found to possess optimum performance when specific capacitance and leakage current considered together. It is also noted that the lattice parameter increases with barium mole fraction. $Ba_{0.7}Sr_{0.3}TiO_3$ ceramic-based MIM capacitor can be made best choice for energy storage application by doping $Ba_{0.7}Sr_{0.3}TiO_3$ ceramic with suitable insulator material to enhance its leakage current performance.

Table 2. Comparison of synthesis and performance parameters with related research works.

Reference	Insulator material	Synthesis method	Calcination temperature/duration (°C/h)	Sintering temperature/duration (°C/h)	Relative permittivity at 1 MHz and at RT	Leakage current (A/cm ²) at 5 V/cm
Balachandran <i>et al.</i> (2011)	Ba _{0.5} Sr _{0.5} TiO ₃	Slow precursor	1100/3	1350/3	550	1 × 10 ⁻⁸
Xiao <i>et al.</i> (2011)	Ba _{0.7} Sr _{0.3} TiO ₃	injection Sol-gel Sol-gel on Si		600/1	Not given	1 × 10 ⁻⁸
Zhu <i>et al.</i> (2012)	Ba _{0.5} Sr _{0.5} TiO ₃	nanoporous pillar array RF magnetron sputtering from powder target			275 at 1 kHz	Not given
Choi <i>et al.</i> (2012)	Ba _{0.7} Sr _{0.3} TiO ₃	Spray pyrolysis	1100/2	1300/2	5500	Not given
Gao <i>et al.</i> (2014)	Ba _{0.6} Sr _{0.4} TiO ₃	Organosol process			874 at 1 kHz	Not given
Battistha <i>et al.</i> (2014)	Ba _{0.9} Sr _{0.1} TiO ₃	Modified Sol gel		750/1	50	Not given
Ćirković <i>et al.</i> (2015)	Ba _{0.8} Sr _{0.2} TiO ₃	Hydrothermally assisted	700/4	1280/16	1125	Not given
Mudinepalli <i>et al.</i> (2015)	Ba _{0.8} Sr _{0.2} TiO ₃	complex polymerization Solid state reaction		1350/2	1500 at 100 kHz	Not given
Attar <i>et al.</i> (2017)	Ba _{0.5} Sr _{0.5} TiO ₃	Sol-gel	850/2	1300/2	420	Not given
Huang <i>et al.</i> (2017)	Ba _{0.4} Sr _{0.6} TiO ₃	Sol-gel and spark	1050/3	1100/3	887 at 100Hz	Not given
Shen <i>et al.</i> (2019)	Ba _{0.3} Sr _{0.7} TiO ₃	plasma sintering Solid state reaction	1200/3	1350/3	650	Not given
This Work	Ba_x Sr_{1-x} TiO₃	Solid state reaction	1100/4	1275/2	2062	6.63 × 10⁻¹⁰

Acknowledgments

The authors are grateful to Dr. Surendran K.P. and his research team from CSIR-National Institute for Interdisciplinary Science and Technology, Thiruvananthapuram, Kerala for help in making green pellets, sintering samples and capacitance measurements.

ORCID

Smitha P. S.  <http://orcid.org/0000-0002-0217-0383>

Jitha S. Jayan  <http://orcid.org/0000-0001-7858-6919>

Appukkuttan Saritha  <http://orcid.org/0000-0002-2253-8050>

V. Suresh Babu  <http://orcid.org/0000-0001-8024-2621>

Shiny G.  <http://orcid.org/0000-0002-8907-9389>

References

1. M. A. Araghi, N. Shaban, and M. Bahar, Synthesis and characterization of nanocrystalline barium strontium titanate powder by a modified sol-gel processing, *Mater. Sci.-Poland* **34** (1), 63 (2016).
2. A. S. Attar, E. S. Sichani, and S. Sharafi, Structural and dielectric properties of Bi-doped barium strontium titanate nanopowders synthesized by solgel method, *J. Mater. Res. Technol.* **6** (2), 108 (2017).
3. W. Cai *et al.*, Vanadium doping effects on microstructure and dielectric properties of barium titanate ceramics, *Ceram. Int.* **37** (8), 3643 (2011).
4. Y. Gao *et al.*, Nanocrystalline barium strontium titanate ceramics synthesized via the “organosol” route and spark plasma sintering, *J. Am. Ceram. Soc.* **97** (7), 2139 (2014).
5. S. M. Olhero, A. Kaushal, and J. M. Ferreira, Fabrication of barium strontium titanate ($\text{Ba}_{0.6}\text{Sr}_{0.4}\text{TiO}_3$) 3D microcomponents from aqueous suspensions, *J. Am. Ceram. Soc.* **97** (3), 725 (2014).
6. R. Balachandran *et al.*, Phase formation and dielectric properties of $\text{Ba}_{0.5}\text{Sr}_{0.5}\text{TiO}_3$ by slow injection solgel technique, *J. Mater. Sci.* **46** (6), 1806 (2011).
7. P. S. Smitha, V. Suresh Babu, and G. Shiny, Investigation of barrier layer effect on performance parameters of Pt/BST/Pt nanocapacitor, *Mater. Res. Express* **6** (9), 094011 (2019).
8. P. S. Smitha, V. Suresh Babu, and G. Shiny, Critical parameters of high performance metal-insulator-metal nanocapacitors: a review, *Mater. Res. Express* **6** (12), 122003 (2019).
9. J. Li *et al.*, Dielectric properties of Barium Strontium Titanate (BST) ceramics synthesized by using mixed-phase powders calcined at varied temperatures, *Mater. Lett.* **76**, 100 (2012).
10. Z. Y. Shen *et al.*, Glass modified barium strontium titanate ceramics for energy storage capacitor at elevated temperatures, *J. Materiom.* **5** (4), 641 (2019).
11. A. Z. Simões *et al.*, Microwave-hydrothermal synthesis of barium strontium titanate nanoparticles, *J. Alloys Compd.* **508** (2), 620 (2010).
12. J. Ćirković *et al.*, Dielectric and ferroelectric properties of BST ceramics obtained by a hydrothermally assisted complex polymerization method, *Ceram. Int.* **41** (9), 11306 (2015).
13. W. Li *et al.*, Solgel synthesis and characterization of $\text{Ba}_{(1-x)}\text{Sr}_x\text{TiO}_3$ ceramics, *J. Alloys Compd.* **499** (2), 255 (2010).
14. S. H. Xiao *et al.*, Structure and ferroelectric properties of barium titanate films synthesized by solgel method, *Mater. Chem. Phys.* **127** (3), 420 (2011).
15. I. K. Batttisha *et al.*, Structural, magnetic and dielectric properties of Fe-Co Co-doped $\text{Ba}_{0.9}\text{Sr}_{0.1}\text{TiO}_3$ prepared by sol gel technique, *NJGC.* **4**, 19 (2014).
16. N. Golego, S. A. Studenikin, and M. Cocivera, Properties of dielectric BaTiO_3 thin films prepared by spray pyrolysis, *Chem. Mater.* **10** (7), 2000 (1998).

17. G. J. Reynolds *et al.*, Sputtered modified barium titanate for thin-film capacitor applications, *Materials (Basel)* **5** (4), 575 (2012). DOI: [10.3390/ma5040575](https://doi.org/10.3390/ma5040575).
18. Z. Xu *et al.*, Dielectric enhancement of BaSrTi_{1.1}O₃/BaSrTi_{1.05}O₃/BaSrTiO₃ multilayer thin films prepared by RF magnetron sputtering, *Ceram. Int.* **39** (2), 1639 (2013).
19. F. Tcheliéou *et al.*, On the microstructure and optical properties of Ba_{0.5}Sr_{0.5}TiO₃ films, *Thin Solid Films* **305** (1–2), 30 (1997).
20. G. Zhu, Z. Yang, and H. Xu, The properties of Ba_{0.5}Sr_{0.5}TiO₃ thin film prepared by RF magnetron sputtering from powder target, *Vacuum* **86** (12), 1883 (2012).
21. P. S. Smitha, V. Suresh Babu, and G. Shiny, VCC- α nullification and leakage reduction in Pt/Ba_{0.5}Sr_{0.5}TiO₃/Pt thin-film capacitor by MgO barrier and PDA for energy storage application, *Semicond. Sci. Technol.* **35** (4), 045004 (2020).
22. A. Khare and N. Chauhan, The effect of Mg doping on structural and luminescent properties of Barium Strontium Titanate (BST), *Phys. Proc.* **76**, 86 (2015).
23. J. Q. Huang *et al.*, Structures and dielectric properties of K and Mg alternately doped BST films, *Integr. Ferroelectr.* **162** (1), 94 (2015).
24. N. Oshima *et al.*, Fabrication and characterization of (110)-oriented (Ba_{0.5}Sr_{0.5})TiO₃ thin films using PdO//Pd buffer layer, *Jpn. J. Appl. Phys.* **54** (10S), 10NA15 (2015). DOI: [10.7567/JJAP.54.10NA15](https://doi.org/10.7567/JJAP.54.10NA15).
25. J. S. J. Hargreaves, Some considerations related to the use of the Scherrer equation in powder X-ray diffraction as applied to heterogeneous catalysts, *Catal. Struct. React.* **2** (1–4), 33 (2016).
26. B. Greenberg, Bragg's law with refraction, *Acta Crystallogr. A Found. Crystallogr.* **45** (3), 238 (1989).
27. Z. Kaszkur, Nanopowder diffraction analysis beyond the Bragg law applied to palladium, *J. Appl. Crystallogr.* **33** (1), 87 (2000).
28. S. H. Choi *et al.*, Dielectric properties of nano-sized Ba_{0.7}Sr_{0.3}TiO₃ powders prepared by spray pyrolysis, *Ceram. Int.* **38** (5), 4029 (2012).
29. V. R. Mudinepalli *et al.*, Effect of grain size on dielectric and ferroelectric properties of nanostructured Ba_{0.8}Sr_{0.2}TiO₃ ceramics, *J. Adv. Ceram.* **4** (1), 46 (2015).
30. J. W. Liou and B. S. Chiou, Dielectric characteristics of doped Ba_{1-x}Sr_xTiO₃ at the paraelectric state, *Mater. Chem. Phys.* **51** (1), 59 (1997).
31. Y. H. Huang *et al.*, Enhanced energy storage properties of barium strontium titanate ceramics prepared by sol-gel method and spark plasma sintering, *J. Alloys Compd.* **701**, 439 (2017).